The formation of Passivation in internally oxidized Ag-based alloys

Ph.D.Ph.D. Jožica Bezjak A. Professor

Abstract—The aim of this research was to analyse the inhibition of internal passivation by changing the chemical composition of silver alloys and to estimate the concentration boundaries of the selected microalloying element at which the passivation is still inhibited. Since, the ability of inoculation or modification is mostly based on the large free energy of formation of oxides of microalloying elements and their crystallographic similarity, Mg in the quantities of 0.001 to 0.5 mass% was chosen as a microalloying element for Ag-based alloys in addition to the main alloying element (Zn). For the Ag-5.8%Zn alloy, the boundary conditions of the inhibition of passivation were established. For concentrations of MgO below 0.005 vol.% not enough nuclei are formed. For too high concentration of MgO (above 1.2 vol.%) defect microstructures are formed which are characteristic for MgO precipitation. This produces a local or general passivation. By changing the composition of microalloying the internal passivation of Ag-5.8%Zn alloy could not only be inhibited but increased. Thus under some microalloying conditions much bigger depths of internal oxidation were reached.

Keywords – Ag-based alloys, Passivation, oxidation kinetics, alloys, microalloying, internal oxidation.

1 INTRODUCTION

The passivation is a phenomenon where at certain depth from the surface of the investigated material an oxide barrier is formed. The formed barrier is thick enough that further progress of oxidation through the material is not possible any more. In internally oxidised alloys the passivation has been observed for certain conditions of concentration of main element, partial pressure and temperature of oxidation[1 to 8]. We attempt to study the inhibition of passivation by microalloying. With the addition of microalloying elements (0.001 to 0.5 mass%) with very high free formation energy of oxides, regarding the oxide of the main alloying element, we tried to inhibit this phenomenon and to enable an undisturbed process of oxidation, as well as a growth of internal oxidation zone.

Our previous investigations[6 to 8] established that Mg, Si, Ti, Al, Zr, Be are important microalloying elements for Ag-Zn, Ag-In and Ag-Sn alloys. These microalloying elements have large affinity to oxygen and therefore oxidise at lower partial pressures (concentrations) of oxygen in silver than the main alloying elements (Zn, In, Sn etc.). Their oxides form the nuclei for the growth of oxides of the main alloying element. Therefore, by their distribution in the metal matrix, the distribution of the main alloying element oxide is also determined (***Fig. 1***)[1,2].

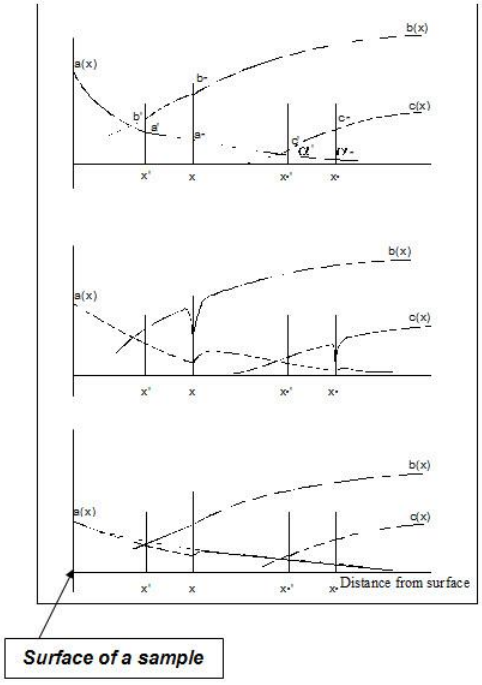

Ph.D.Ph.D. Jožica Bezjak A. Professor, University of Primorska, PEF, President of Association of Technical CreativenessEducatorsSlovenia, jozica.bezjak2@gmail.com

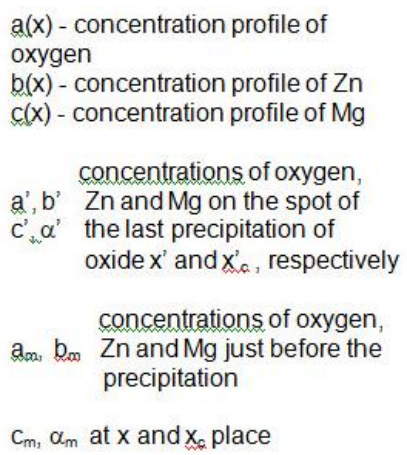

Fig. 1
The scheme of the concentration profile of oxygen and alloying elements at the beginning of the internal oxidation zone.

This heterogeneous nucleation is very effective at the defined concentration interval of a microalloying element.
The aim of our research was to analyse the inhibition mechanism of the formation of passivation in the Ag-Zn alloys by changing the fraction of main alloying element, as well as the fraction of microalloying element (Mg) and to estimate the range of concentrations at which the microalloying element Mg is still effective as a modificator.

2 EXPERIMENTAL

The different alloys (***Table 1***) were prepared in evacuated (up to 10^{-2} bar) quartz tubes in an induction furnace. After 30 hours of homogenisation and annealing at 800 °C the alloys were hot forged and recrystallization annealed. Finally, they were cold rolled into 3 mm thick stripes, which were then ground and etched in 10 % solution of HNO_3.

Main alloying element Zn	**Type of oxide ZnO**	**Additional alloying element**	**Types of oxides MgO**	**Alloy designation**
mass% at%	mass% vol.%	mass% at% **of Mg**	mass % vol. %	
6.3 (9.97)	7.74 (13.73)			2S1
0.045 (0.20)	0.08 0.217 (MgO)			2S0
5.8 (9.18)	7.12 (12.64	0.51 (2.29)	0.85 2.46	3S1
5.8 (9.18)	7.12 (12.64)	0.29 (1.31)	0.48 1.39	3S2
5.0 (7.91)	6.14 (10.89)	0.25 (1.18)	0.43 1.20	1S4
5.8 (9.18)	7.12 (12.64)	0.21 (0.95)	0.35 1.01	2S2
5.8 (9.18)	7.12 (12.64)	0.065 (0.29)	0.108 0.31	2S3
5.8 (9.18)	7.12 (12.64)	0.012 (0.05)	0.02 0.06	3S3
5.0 (7.91)	6.14 (10.89)	0.001 (0.005)	0.002 0.005	1S6
5.8 (9.18)	7.12 (12.64)	<0.002 (0.009)	0.003 0.009	2S4
5.8 (9.18)	7.12 (12.64)	0.001 (0.005)	0.002 0.005	3S4

Table 1 *Chemical composition of the investigated Ag-based alloys*

The tests of internal oxidation kinetics were made at different temperatures (in the temperature range between 750 °C and 850 °C), and at different time (from 5 to 140 hours) in a tube furnace, where air flow circulation was assured.
In the most cases, the oxidising atmosphere was air. However, some tests, in the oxidising atmosphere of oxygen (with partial pressure of 1.01×10^5 Pa) were also performed.
Microstructural changes in the zone of internal oxidation were observed by optical (Leitz Wetzlar, Germany and Nikon Microphot–FXA, Japan) and scanning electron microscopy (SEM/WDX analyser Jeol JSM 840 A). Volume and energy changes, as well as the process of internal oxidation were measured by thermogravimetric analysis (TGA, Mettler TG 50,

Germany). Applying the Wagner's theory[1 to 3], the changes of system kinetics were calculated.

3 RESULTS

The distributions of Ag, Mg, and Zn in the region of internal oxidation zone and in the non-oxidised part of investigated alloys were observed (***Fig. 2***) and analysed by the electron probe X-ray microanalyzer (EPMA; Jeol JXA 3A).

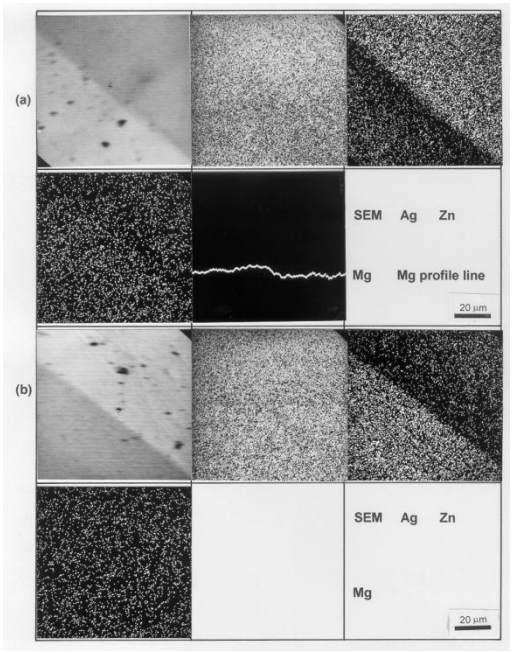

Fig. 2
a *to* ***b*** *Distributions of Ag, Zn and Mg at the transition between internal oxidation zone and nonoxidised alloy; 830 °C/20 h/air,* ***(a)*** *2S2 and* ***(b)*** *2S3 alloys (obtained by EPMA profile and mapping analysis; Jeol JXA 3A).*

*In the front of the internal oxidation zone a stripe with lower concentration of Zn can be noticed. This is evident from the concentration profile of Zn in the internal oxidation zone (****Figs 3a*** *and* ***b****). The differences in the concentration, as well as a distribution of Mg in both studied alloys were also determined.*

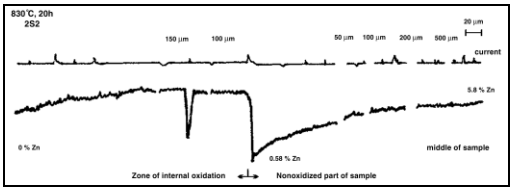

Fig. 3a*: Concentration profile of Zn, in the sample of 2S2 alloy, microalloyed with 0.21% Mg, through the internal oxidation zone and to the middle part of the non-oxidised sample (obtained by EPMA profile analysis; Jeol JXA 3A).*

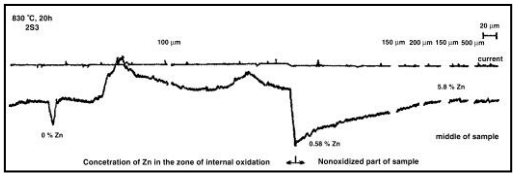

Fig. 3b *Concentration profile of Zn in the sample of 2S3 alloy, microalloyed with 0.065% Mg, through the internal oxidation zone and part of the non-oxidised sample towards the middle of the sample (obtained by* EPMA profile *analysis; Jeol JXA 3A).*

The results of measurements in the zone of internal oxidation and at the beginning show that the average concentrations of Zn are significantly higher than its starting concentration in the alloy. In the 2S3 alloy, the spots with slightly higher concentrations at crystal boundaries and at other defects in the alloy were observed which is the evidence of an improper concentration of microalloying element Mg. The measurements of microhardness also confirmed the measured values of concentration profiles (see ***Figs 4a*** and ***b***) because the hardness is increased with increased content of oxide particles.

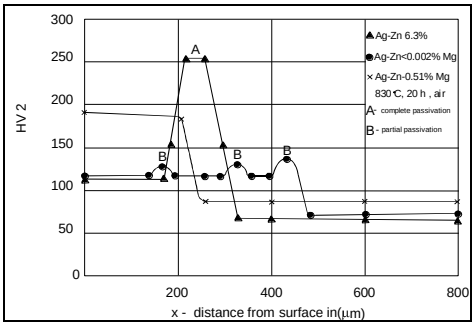

Fig. 4a *Dependence of Vickers hardness HV2 (load 20N, Zwick hardness tester, Model Z323, Germany) and distance from the sample surface at 2S1, 2S4 and 3S1 alloys.*

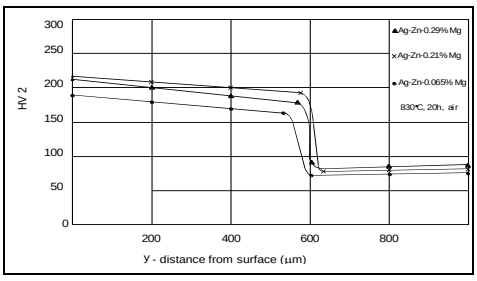

Fig. 4b *Dependence of Vickers hardness HV2 and the distance from the sample surface at differently modified alloys (3S2, 2S2, 2S3).*

The rate of internal oxidation zone displacement (***Fig. 5***) and the mass changes of internally oxidised AgZnMg alloys measured by TGA were used to determine the reaction kinetics of the internal oxidation.

There are several equations in the literature[1 to 2] how to calculate the distance of internal oxidation zone from the sample's surface. The kinetics constant for the parabolic growth of the internal oxidation zone was calculated by the help of experimental TGA data of isothermal measurements. The equation:

$$(\Delta X)^2 = Kt \quad \textbf{(1)}$$

was adapted as follows:

$$(\Delta m)^2 = Kt \quad \textbf{(2)}$$

where in the **equations (1)** and **(2)** are:

x ….. depth of internal oxidation zone (m)
K ….. kinetics constant of internal oxidation ($m/s^{2)}$
t ….. oxidation time
m …. mass of formed oxide

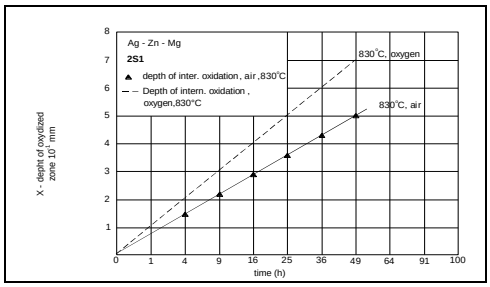

Fig. 5 *Growth kinetics of internal oxidation zone of AgZnMg alloy, oxidised in air and in the atmosphere of oxygen.*

The activation energy was derived with the Arrhenius equation[2]:

$$\ln K = \ln K_0 - E_a / RT \quad \textbf{(3)}$$

where in the **equation (3)** are:

K_0 ….. parametric constant of internal oxidation ($m/s^{2)}$
E_a ….. activation energy (for volume diffusion of oxygen)
R …… gas constant (8.31 kJ/kmol·K)
T …..... absolute temperature (K)

Taking into account the dependence of logarithm of the reaction rate constant from the reciprocal value of the temperature (**Fig. 6, Table 2**), the value of E_a for the alloy with optimal composition (2S2) was determined: **E_a = 103 ± 4,8 kJ/mol**

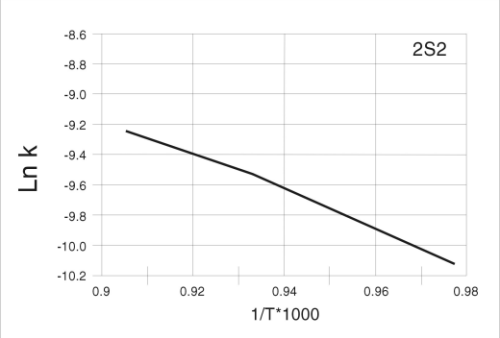

Fig. 6 *Dependence of kinetics constant from reciprocal value of temperature for the 2S2 alloy.*

T(°C)	lnK	1/T·10³
750	-10.1058	0.977517
800	-9.5095	0.931966
830	-9.2342	0.906618

Table 2 Logarithmic values of reaction constant rate of 2S2 alloy

4 DISCUSSION

The results of kinetics, the investigations with electron probe microanalyzer and optical microscopy, as well as the measurements of hardness confirmed the correct selection of alloys. The alloying with Mg in the quantities of 0.001 to 0.25 mass% the passivation was inhibited, and undisturbed growth of internal oxidation zone was achieved.

Our investigations proved that the inocculation ability depends on the discrepancy of free energy of oxide formation and crystallographic similarities of oxides. And because the oxide with high free energy of formation is formed much earlier than the oxide with lower free energy of formation, it can serves as a nucleus (***Figs 7a*** to ***d***). At this kind of inocculation characteristic for ternary alloys, there are two

kinds of oxides formed at different times at the determined location. The oxide with high free formation energy forms earlier and its particles are always thinner and better dispersed (***Fig. 7a***). ZnO later form the precipitates on them (***Fig. 7b***). Thus primary thin particles in our Zn oxides alloys serve as heterogeneous nuclei which makes the precipitation of secondary oxides easier.

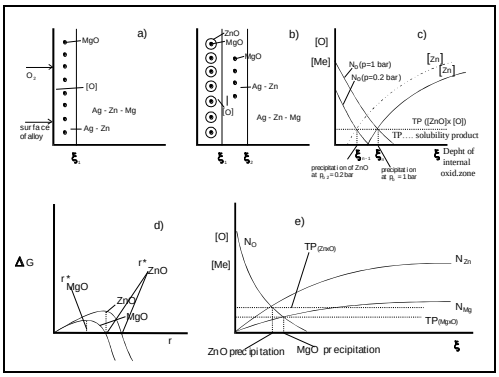

Figs 7a to ***e*** *Scheme of internal oxidation of Ag-Zn alloy, modified with Mg:* ***(a)*** *oxidation of Mg and formation of MgO,* ***(b)*** *oxidation of Zn and ZnO precipitation on MgO,* ***(c)*** *the distribution of oxygen concentration in the dependence of partial pressure of oxygen in the atmosphere,* ***(d)*** *the size of MgO and ZnO nuclei,* ***(e)*** *the difference on the spot of MgO and ZnO precipitation in the dependence of the location, where the solubility product of both oxides was achieved.*

The inocculation also causes the set of changes. These changes depend on the size, shape, distribution and dispersion of oxides of the main alloying element in the alloy. Comparing the precipitation of oxides in binary alloys (***Fig. 8***) with the precipitation of oxides in modified ternary alloys (***Figs 9a*** to ***c*** and ***Fig. 10***), one can conclude that at the latter the distribution of oxide particles is much more uniform and regular and therefore totally inhibits the passivation.

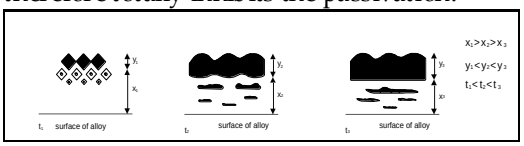

Fig. 8 *Scheme of the formation of oxide barrier in binary alloy at 830 ^{0}C and at different times of oxidation.*

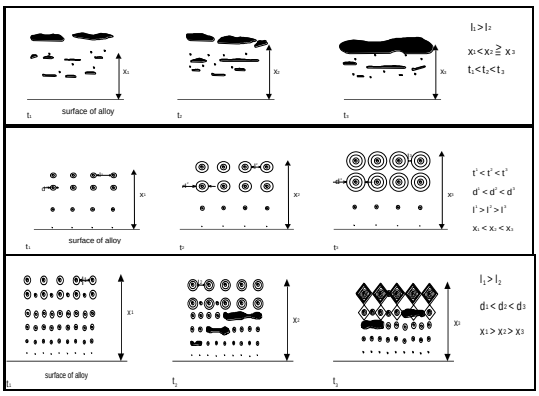

Fig. 9 *Scheme of distributions of oxide particles in modified ternary alloys at 830 ^{0}C and at different times of oxidation:* ***(a)*** *with too low,* ***(b)*** *adequately,* and ***(c)*** *too high concentration of microalloying element;* ***l_1, l_2, l_3*** *distance between oxide particles;* ***d_1, d_2, d_3*** *diameter of oxide particles;* ***x_1, x_2, x_3*** *distance of oxide zone from the surface of the sample;* ***t_1, t_2, t_3*** *internal times of oxidation (5, 25, 50 h).*

From the microstructure of internal oxidation zone shown in metallographic images (see ***Figs 10*** to ***15***), it is evident that the lowest concentration limit of the microalloying element Mg, which already acts as an inoculant, is approximately 0.001 mass% and the highest concentration limit is approximately 0.25 mass%. The addition of Mg above upper limit increases the fraction of defect microstructural elements in the internally oxidised zone and thus it alone provokes partial or even total passivation.

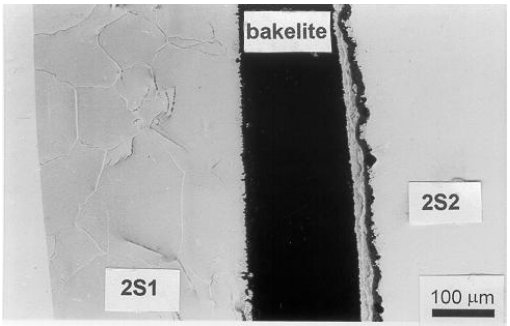

Fig. 10 *Optical microscope micrograph of Internally oxidised zone in the 2S1 alloy (left), and in the 2S2 alloy (right); 830 ^{0}C/20h/air, left: occurrence of passivation, right: no passivation, larger depth of int. oxidation.*

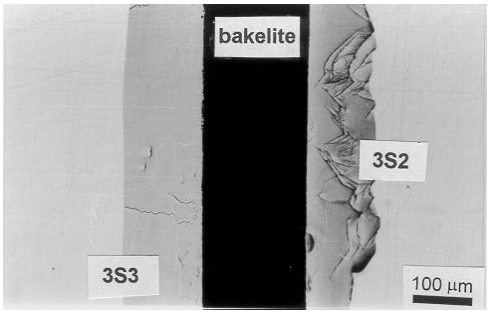

Fig. 11 *Optical microscope micrograph of internally oxidised zone in the 3S3 alloy (right) and in the 3S2 alloy (left); 830 °C/20 h/air, only partial passivation is noticed, complete passivation has not happened still.*

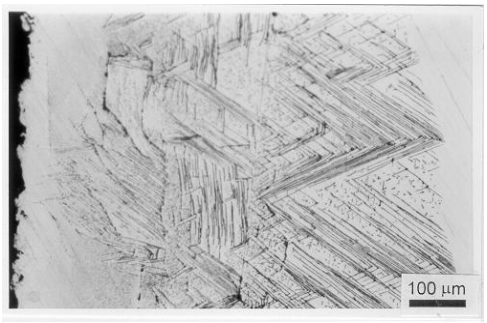

Fig. 12 *Optical microscope micrograph of internally oxidised zone in the 1S6 alloy; 830 °C/20 h/air, fine needle-like oxide particles like pearlite structure are formed because of higher concentration of Mg.*

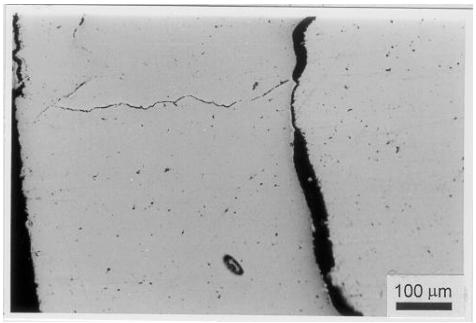

Fig. 13 *Optical microscope micrograph of internally oxidised zone and the formation of the main oxide barrier in the 3S2 alloy; 830 °C/20 h/air, passivation has occurred because of too high concentration of Mg*

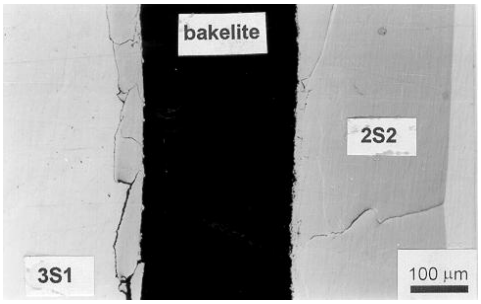

Fig. 14 *Optical microscope micrograph of internally oxidised zone in the 3S1 (left) and 2S2 alloy (right); 830 °C/20 h/air, larger depth of internal oxidation because of the appropriate concentration of Mg .*

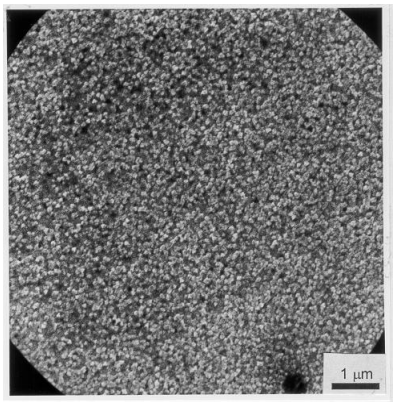

Fig. 15 *SEM micrograph of oxide particles distribution in the 2S3 alloy; 830 °C/20 h/air, 50 µm from the surface of the sample.*

5 CONCLUSIONS

On the basis of our research it was found out that the size and distribution of oxide particles in the selected AgZnMg alloys depend on temperature and partial pressure of oxygen, as well as on the concentration of microalloying element. It was also established that the inoculation weakens by the increased temperature and partial pressure of oxygen. The most convenient conditions for inoculation occurs at the appropriate number of nuclei. The corresponding concentration of microalloying element is between 0.001 and 0.25 mass% of Mg. On the other side, either too low (0.001 mass%) or to high (0.25 mass%) concentration of oxide nuclei causes the formation of larger oxide particles (polyhedrons, needles and lamellas). Too large concentration of microalloying element leads directly to passivation.

The mechanism for the successful nucleation in modified silver based alloys is based on the sufficient number of nuclei of oxide particles of microalloying element which are uniformly dispersed in metal matrix and cause the prolongation of ZnO precipitation.

REFERENCES

[1] Wagner, C.: Z. Elektrochem, 63(1959), 772.
[2] Böhm, G.; Kahlwait, M.: Acta metall., 12(1964), 641-648.
[3] Hauffe, K.: Reaktionen in und an festen Stoffen, Springer Verlag, Berlin(1955).
[4] Stöckel, D.: Kinetik der inneren Oxydation von Silber-Aluminium-Legierungen, Metall, 7(1971), 755-760.
[5] Rapp, R.A.: Acta metall., 9(1961), 730-441.

[6] Bezjak, J.: Ph. D. Dissertation, University of Ljubljana, Slovenia(1995).
[7] Bezjak, J.: B.Sc. work, University of Ljubljana, Slovenia(1986)
[8] Bezjak, J.; Kosec, L.: Z. Metallkd. 90(1999), 159.
[9] R.A Rapp, D.F Frank, J.V Armitage *Acta Metallurgica*, *Volume 12, Issue 5*, *May 1964*, *Pages 505-513*
[10] Nicholas Winograd, W. E. Baitinger, J. W. Amy and J. A. MunarinVol. 184 no. 4136 pp. 565-567 DOI: 10.1126/science.184.4136.565
[11] V.A van Rooijen‡, E.W van Royen‡, J Vrijen‡, S Radelaar†, 2003.
[12] C.P. Wu, D.Q. Yi, J. Li, L.R. Xiao, B. Wang, F. Zheng. Journal of Alloys and Compounds, Volume 457, Issues 1-2, 12 June 2008, Pages 565-570.
[13] Juan F. García Martín, Sebastián Sánchez and Renaud Metz, 2011. Kinetics Model of the Thermal Oxidation of Indium Powder.
[14] G. Korotcenkov, The role of morphology and crystallographic structure of metal oxides in response of conductometric-type gas sensors, Mater. Sci. Eng. R 61 (2008) 1-39.
[15] E. Comini, C. Baratto, G. Faglia, M. Ferroni, A. Vomiero, G. Sberveglieri, Quasi-one dimensional metal oxide semiconductor: preparation, characterization and application as chemical sensors, Prog. Mater. Sci., (In Press), Available online 10 July 2008.
[16] A. Kolmakov, X. Chen, M. Moscovits, Functionalizing nanowires with catalytic nanoparticles for gas sensing applications, J. Nanosci. Nanotech. 8 (2008) 111-121.
[17] M. Tiemann, Porous Metal Oxides as Gas Sensors, Chem. Eur. J. 13 (2007) 30, 8377-8388
[18] G. Korotcenkov, Metal oxides for solid state gas sensors. What determines our